Korean J. Chem. Eng., 38(2), 442-453 (2021)
DOI: 10.1007/s11814-020-0616-0

pISSN: 0256-1115
eISSN: 1975-7220

Nature-mimicking fabrication of antifouling photocatalytic membrane based on Ti/BiOI and polydopamine for synergistically enhanced photocatalytic degradation of tetracycline

Yanhua Cui*, Lili Yang*, Yan Yan*, Zengkai Wang*, Jian Zheng**, Binrong Li***, Yonghai Feng*, Chunxiang Li**,†, and Minjia Meng**,†**

*School of Materials Science and Engineering, Jiangsu University, Zhenjiang 212013, China
**Institute of Green Chemistry and Chemical Technology, School of Chemistry and Chemical Engineering, Jiangsu University, Zhenjiang 212013, China
***School of Environment and Safety Engineering, Jiangsu University, Zhenjiang 212013, China
(*Received 12 November 2019 • Revised 18 May 2020 • Accepted 30 June 2020*)

Abstract−The photocatalytic efficiency of conventional blending photocatalytic membranes suffers a significant reduction due to effective photocatalyst embedded in membrane matrix. Therefore, in this study, inspired by the bioadhesive technology of polydopamine (pDA), a novel Ti doped bismuth oxyiodide (BiOI)-polydopamine (pDA)-coated cellulose acetate (CA) (Ti/BiOI-pDA/CA) photocatalytic nanocomposite membranes were successfully developed for effective removal of tetracycline (TC). The Ti/BiOI-pDA/CA nanocomposite membranes displayed very high photocatalytic activity toward TC (about 98% after 120 min) under visible light irradiation and superior photodegradation kinetics ($k=0.03214\ min^{-1}$). The removal rate of Ti/BiOI/-pDA/CA nanocomposite membranes under dynamic cyclic degradation system could be further improved, giving TC removal efficiency of 91% in 60 min. Remarkably, the permeate flux, flux recovery ratio (FRR), reversible fouling (Rr), irreversible fouling (Rir) and the total fouling ratio (Rt) revealed the Ti/BiOI-pDA/CA nanocomposite membranes had excellent antifouling performance. In addition, the Ti/BiOI-pDA/CA nanocomposite membranes exhibited excellent stability and reusability. Therefore, this work gives insight into the effective removal of TC wastewater and has a great potential for new generation of high-performance photocatalytic membranes for practical wastewater treatment in the future.

Keywords: Flower-like Ti/BiOI, pDA/CA Hybrid Membrane, Fouling Mechanismm Photodegradation

INTRODUCTION

Tetracycline (TC), as an efficient broad-spectrum antibiotic, is frequently used in the treatment of human and animal bacterial infections [1]. However, the widespread use and abuse of TC readily leads to the generation of its residues in dairy food products and waste water. Even a low concentration of TC residues in aquatic media can affect the dynamic balance of bacterial population and promote the spread of antibiotic-resistant bacteria, which further poses enormous threats to the aquatic ecosystem balance and human health [2,3], including nephropathy, gastrointestinal reactions, mutagenic and teratogenic effects [4-6]. Therefore, it is necessary to develop an efficient and convenient technique to remove TC from environmental wastewater.

Tremendous efforts have been devoted to developing advanced technologies for efficient removal of TC from wastewater, such as adsorption, photocatalytic degradation and membrane separation [7-9]. Among these, membrane separation has been considered as a promising technology due to its high efficiency and low energy consumption in wastewater treatment [10]. However, during the separation process, a conventional membrane usually suffers from deposition of contaminant such as proteins and micro-organisms, which will block the membrane surface and pores and result in membrane fouling [11,12]. To overcome these obstacles, the incorporation of photocatalyst into membranes to prepare photocatalytic membranes will simultaneously degrade TC and other organic contaminants [13,14]. Additionally, these photocatalytic membranes can be easily reused, which can enlarge industrial application [15-17]. Xu et al. [18] developed GO/TiO_2-PVDF nanocomposite membranes to achieve high photodegradation efficiency and excellent self-cleaning performance under UV illumination. Zhang et al. [19] prepared Ag/β-CD/PAN-TiO_2 photocatalytic membrane with adsorption capacity, degradation and self-cleaning property. These photocatalytic membranes were prepared by blending method, which dramatically solves the problem of membrane fouling. However, there is an inevitable defect of the above blending method that a number of "effective photocatalysts" have been embedded in membrane matrix and the accessible catalytic sites will be reduced during the membrane fabrication process [20,21]. Therefore, it is highly important to solve the embedding problem of photocatalyst in the membrane matrix and further improve the catalytic properties of nanocomposite membranes.

To address the above issues, the critical step is to construct a highly efficient photocatalyst first. Bismuth oxyhalides, among the most

†To whom correspondence should be addressed.
E-mail: lcx@mail.ujs.edu.cn, mmj@ujs.edu.cn

promising photocatalysts, have been systematically studied due to their high photocatalytic ability [22-24]. Among these photocatalysts, BiOI has received extensive attention due to its high photocatalytic activity, nontoxicity and environmental friendliness. BiOI displays a layer structure consisting of positive $[Bi_2O_2]^{2+}$ sheets and negative I-slabs; this unique structure is beneficial to the effective separation of photogenerated electron-hole pairs [25,26]. Recently, many strategies have been proposed to further improve the photocatalytic performance of BiOI by modification of BiOI with doping (C) [27], or with semiconductor (g-C_3N_4, NiO and $SrTiO_3$ coupling [28-30], morphology control [25,26], and loading with noble metals [31]. The appropriate amount of Ti doping BiOI (Ti/BiOI) can enhance photocatalytic and antibacterial properties owing to the good photo-electron response of Ti. For instance, Tong et al. [32] constructed Ti doped BiOI microspheres, significantly enhancing the antibacterial activities under visible light irradiation. Especially, flower-like Ti/BiOI photocatalyst has a larger specific surface area, which is beneficial to adsorption and degradation. However, no prior work regarding the photocatalytic performance of flower-like Ti/BiOI based nanocomposite membranes has been reported.

On the basis of high-efficiency photocatalysts, how to effectively couple membrane with photocatalysts is another key step of constructing blending photocatalytic membranes. Polydopamine (pDA) has been widely applied due to its strong bioadhesive performance and outstanding biocompatibility, which can form a thin layer coating on almost any solid substrate surface in mild alkaline aqueous solution [33-36]. Recently, researchers have developed photocatalytic membranes by surface modifying the substrate membrane with pDA, then the photocatalysts are stabilized on the surface of the pDA-coated membrane. For example, Wang et al. successfully prepared pDA-coated poly(vinylidene fluoride) (pDA/PVDF) membrane, then Au-TiO_2 photocatalyst was vacuum-filtered on the surface of pDA/PVDF membranes to enhance photocatalytic activity [37]. Although this method solved photocatalyst embedding problems existing in the traditional blending photocatalytic membranes, it still suffered from the agglomeration or leakage of photocatalysts or blocking of pores or surface damage or collapse, and even causing secondary pollution. Self-assembly of dopamine onto the polymer matrix material directly is an alternative way to address these drawbacks, and the N-H and catechol groups of pDA give it an active site for immobilizing metal ions [38-41]. Coincidentally, Ti/BiOI photocatalysts could be easily immobilized on the surface of the pDA by strong coordination bonds, which is conducive to the uniform deposition of Ti/BiOI photocatalysts on both the surfaces and cross-section of the membrane. In addition, researchers also report that pDA possesses a strong light harvesting ability and good electrical conductivity, which can greatly enhance the optical and electrical properties of matrix materials [42,43]. Importantly, pDA as electron and proton acceptor can inhibit the electron-hole recombination of photocatalysis and improve photocatalytic activity [44,45].

In this study, a facile and versatile approach for the preparation of Ti/BiOI-pDA/CA nanocomposite membranes by the generation in situ and phase inversion method was reported and applied to degrade TC under visible light irradiation. pDA can maximize the uniform distribution of photocatalysts on the surfaces and channels of the membrane, which accelerates transfer and separation ability of the photogenerated charge carriers inside the membrane and further effectively improves photocatalytic efficiency. The morphological structure of Ti/BiOI-pDA/CA nanocomposite membranes was characterized by X-ray diffraction (XRD), scanning electron microscopy (SEM), Fourier transform infrared (FT-IR), atomic force microscopy (AFM) and X-ray photoelectron spectroscopy (XPS). The effect of addition of Ti/BiOI on CA or pDA/CA membranes was investigated by examining filtration performance, fouling resistance and photocatalytic property by the photodegradation of TC under dynamic cyclic/static degradation system. It is expected that the Ti/BiOI-pDA/CA nanocomposite membranes would be an attractive material for further practical industrial application.

EXPERIMENTAL SECTION

1. Materials

Cellulose acetate (CA), dimethyl sulfoxide (DMSO), bismuth nitrate pentahydrate ($Bi(NO_3)_3{\cdot}5H_2O$), potassium iodide (KI) and absolute ethyl alcohol (C_2H_5OH) were purchased from Sinopharm Chemical Reagent Co., Ltd, China. Tris(hydroxymethyl)aminomethane hydrochloride (Tris-HCl), titanium butoxide ($C_{16}H_{36}O_4Ti$), ammonium hydroxide ($NH_3{\cdot}H_2O$), dopamine hydrochloride (DA) were supplied by Aladdin, Shanghai. Doubly distilled water was used in all cleaning process and aqueous solutions in the experiments.

2. Method

2-1. Modification of CA by Self-polymerization of DA

pDA/CA was synthesized by self-polymerization of DA at room temperature. In a typical procedure, the purified CA power (6.0 g) was first immersed into 300 mL mixed solution including 0.1815 g of Tris-HCl and 0.3 g of DA. The self-polymerization of DA was initiated by alkaline conditions (pH=8.5). Then the reaction system was stirred for 6.0 h. The obtained pDA modified CA (pDA/CA) was subsequently collected and rinsed with plenty of DI water to remove any unreacted residues before being dried under vacuum at 40 °C.

2-2. Synthesis of Ti-doped BiOI Photocatalyst

Ti-doped BiOI photocatalysts were synthesized by a one-pot solvothermal process. In a typical procedure, 0.485 g (1.0 mmol) $Bi(NO_3)_3{\cdot}5H_2O$ was dissolved in 20 mL of absolute ethanol and ultrasonicated for 30 min. 0.166 g (1.0 mmol) KI was dissolved into 20 mL deionized water, then this aqueous solution was dropwise injected into the above-mentioned mixture under vigorous stirring for 1.0 h; 400 μL of $C_{16}H_{36}O_4Ti$ was added into the above mixed solution. Stirring followed for another 0.5 h. Finally, the obtained solution was transferred into a Teflon-lined autoclave (50 mL) to undergo a solvothermal process at 180 °C for 2.0 h. The obtained precipitates were collected and washed with deionized water and absolute ethanol for three times, respectively, and dried in an oven at 60 °C in air. Pure BiOI samples were also prepared in the same way as the Ti/BiOI photocatalyst with the absence of $C_{16}H_{36}O_4Ti$.

2-3. Preparation of Ti/BiOI-pDA/CA Nanocomposite Membranes

To prepare Ti/BiOI-pDA/CA nanocomposite membranes, initially a predetermined amount of Ti/BiOI photocatalyst was mixed separately with DMSO solvent and kept under ultra-sonication for 0.5 h to attain the complete dispersion of Ti/BiOI in the solvent.

Table 1. Membrane composition for all nanocomposite membranes

Membrane	CA (wt%)	Photocatalyst	(wt%)	DMSO (wt%)
CA	13	-	-	87
pDA	13	-	-	87
BiOI-CA	11	BiOI	2	87
BiOI-pDA/CA	11	BiOI	2	87
Ti/BiOI-CA	11	Ti/BiOI	2	87
Ti/BiOI-pDA/CA	11	Ti/BiOI	2	87

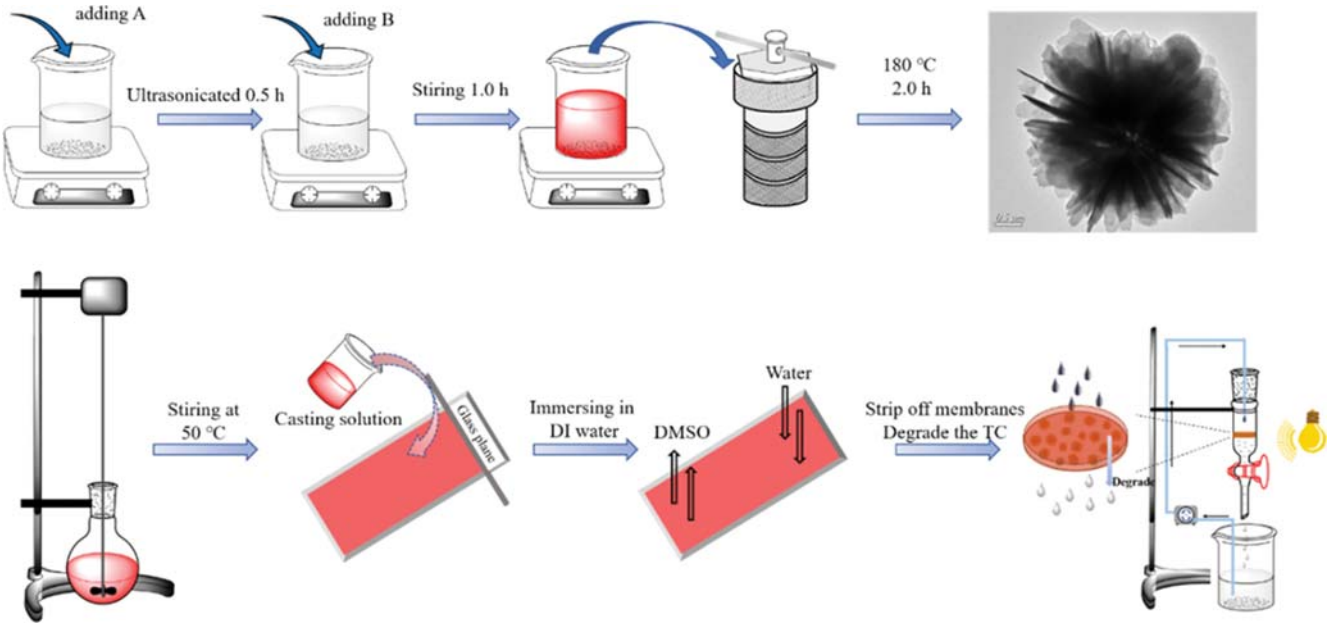

Fig. 1. Schematic illustration for the preparation process of nanocomposite membranes.

Then the pDA/CA was mixed with the above obtained homogeneous mixture and stirred for 10 h at 50 °C and then stored for another 4.0 h to remove the air bubbles. The as-prepared solution was then cast on an undefiled glass plate using a doctor knife, then instantly immersed in a coagulant bath containing deionized water. For comparison, the polymer, additive and solvent blend composition of pure CA, pDA/CA and Ti/BiOI-pDA/CA nanocomposite membranes are given in Table 1. All the above-mentioned preparation process is summarized and presented in Fig. 1.

2-4. Characterization

The crystal structure, phase purity, morphology, surface analysis and roughness of the prepared membranes were characterized by X-ray diffraction (XRD, Rigaku, operated at 40 kV and 200 mA, Cu Kα source, 7.0° min^{-1}, 2θ range from 10 to 80°), field-emission scanning electron microscope (FE-SEM, JSM-6010PLUS/LA), X-ray photoelectron spectroscopy (XPS) and atomic force microscope (AFM, Agilent PicoPlus), respectively. The functional groups of different membranes were identified using Fourier transform spectrophotometry (FT-IR, Nexus 470, Thermo Electron Corporation).

2-5. Membrane Performance Tests

The porosity of the membranes was evaluated by using gravimetric method in the following equation [46] (Eq. (1)):

$$\varepsilon = \frac{\frac{W_w - W_d}{\rho_w}}{\frac{W_w - W_d}{\rho_w} + \frac{W_d}{\rho_P}} \times 100 \quad (1)$$

where W_w is the weight of wet membranes and W_d is the weight of the dry membranes (g). ρ_w and ρ_p are the density of water (0.998 g cm^{-3}) and CA (1.3 g cm^{-3}), respectively.

2-6. Filtration and Fouling Study of Membranes

The antifouling performance of the membranes was assessed with a static bovine serum albumin (BSA) adsorption test according to our previous report [47].

The pure water flux and fouling analysis measurements were measured with an effective area of 3.14 cm^2 using a dead-end cell under 0.8 bar [48]. The water flux of the prepared membranes was evaluated by Eq. (3):

$$J = \frac{V}{S \cdot \Delta t} \quad (2)$$

where J is the pure water flux of the membranes (L m^{-2} h^{-1}), V is the volume of pure water (L), S and Δt are the area of the membranes (m^2) and the time (h), respectively.

To further evaluate the anti-fouling property of the membranes,

four parameters were introduced. First, the pure water flux was measured at 0.8 bar (J_1), subsequently BSA (1.0 g/L) was chosen as the model foulants and the foulant solution flux was continuously monitored for 30 min (Jp) under the same pressure. Finally, the pure water flux was measured again (J_2). The flux recovery ratio (FRR), the total fouling ratio (Rt), irreversible fouling ratio (Rir) and reversible fouling ratio (Rr) were calculated as follows, Eqs. (3)-(6), respectively:

$$FRR = \left(\frac{J_2}{J_1}\right) \times 100 \tag{3}$$

$$R_t = \left(1 - \frac{J_P}{J_1}\right) \times 100 \tag{4}$$

$$R_r = \left(\frac{J_2 - J_P}{J_1}\right) \times 100 \tag{5}$$

$$R_{ir} = \left(\frac{J_1 - J_2}{J_1}\right) \times 100 \tag{6}$$

RESULTS AND DISCUSSION

1. Structural and Morphological Analyses of Ti/BiOI Photocatalyst

The crystal structure and phase composition of BiOI and Ti/BiOI samples were carried out on X-ray diffraction (XRD), and the results shown in Fig. 2. For the BiOI sample, the major reflection

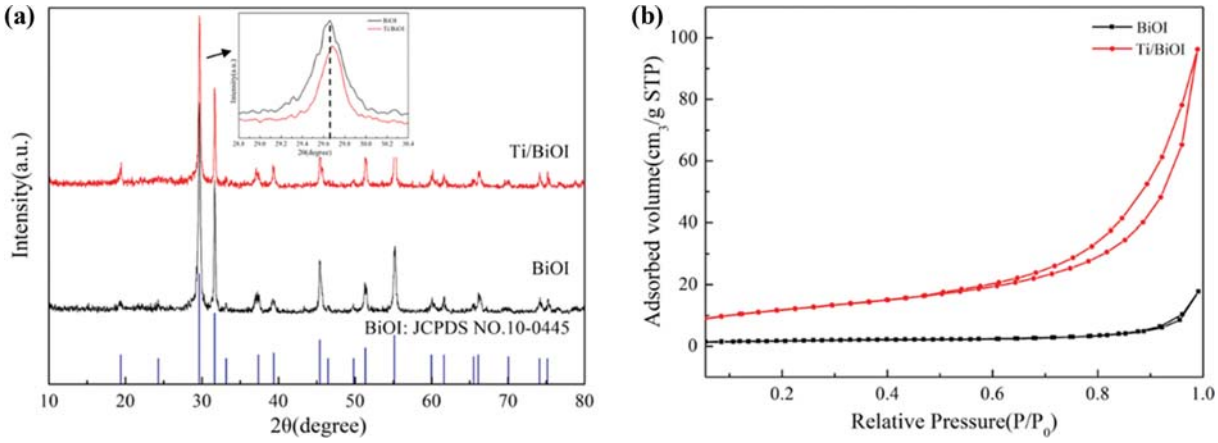

Fig. 2. (a) XRD patterns and (b) the BET analysis of the as-prepared BiOI and Ti/BiOI.

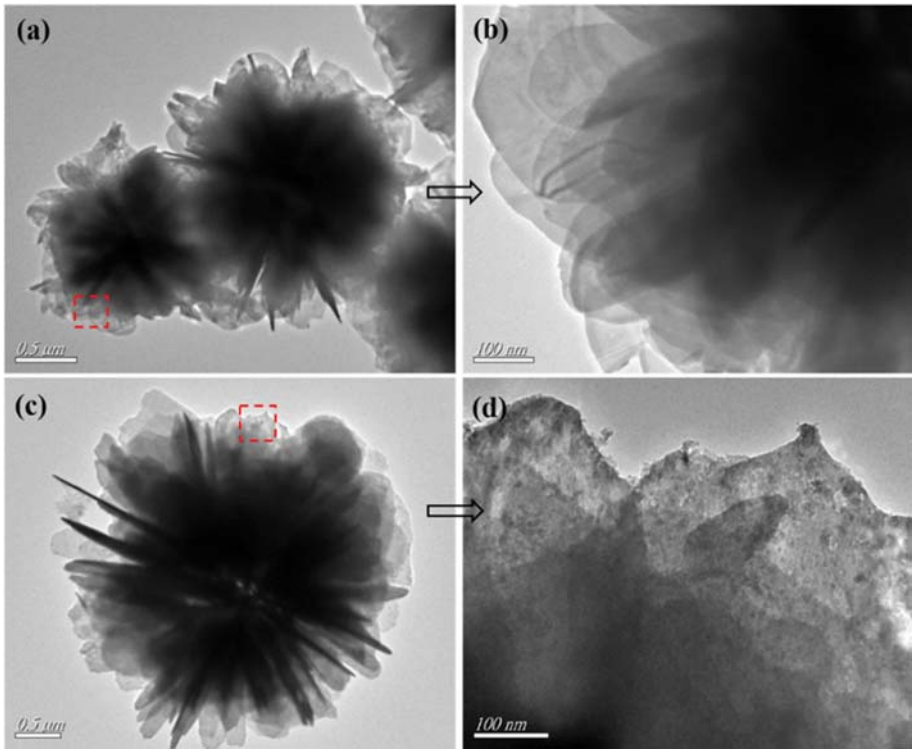

Fig. 3. TEM images of (a), (b) BiOI and (c), (d) Ti/BiOI.

peaks were situated at 2θ=29.6°, 31.7°, 37.4°, 39.4°, 45.7°, 51.3° and 55.2°, which could be assigned to the (102), (110), (004), (112), (200), (114) and (212) planes of bismuth oxide iodide (JCPDS No. 10-0445). However, the diffraction patterns of Ti/BiOI showed similar weak peaks and a slight shift in peak intensity of (102) peak could be observed (inset of Fig. 2(a)). This phenomenon could be ascribed to the fact that the Ti^{3+} ions may embed in the lattice of BiOI [33]. The result indicated Ti/BiOI could be successfully prepared by one-pot solvothermal method.

The N_2 adsorption-desorption isotherm measurement of the prepared BiOI and Ti/BiOI photocatalyst was used to determine the adsorption capacity toward TC. According to the results in Fig. 2(b), the BET specific surface areas of the BiOI and Ti/BiOI were 6.2930 $m^2\ g^{-1}$ and 41.8832 $m^2\ g^{-1}$, respectively. The high specific surface area of the Ti/BiOI would provide more reaction sites than that of the BiOI. Therefore, the photocatalytic activity of the Ti/BiOI sample was enhanced obviously.

The microstructures of the as-synthesized samples were further investigated by TEM. As seen in Fig. 3(a) and 3(c), BiOI and Ti/BiOI show flower-like morphology. No critical morphology change was observed after Ti doping. In Fig. 3(d), the Ti species are well anchored on the surface of the BiOI substrate. The above results

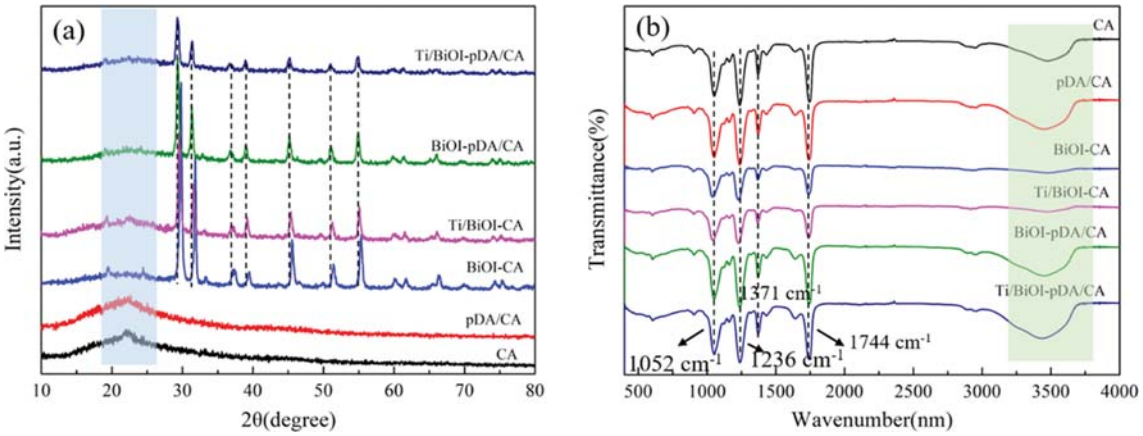

Fig. 4. (a) XRD patterns, (b) FTIR spectra of as-prepared membranes.

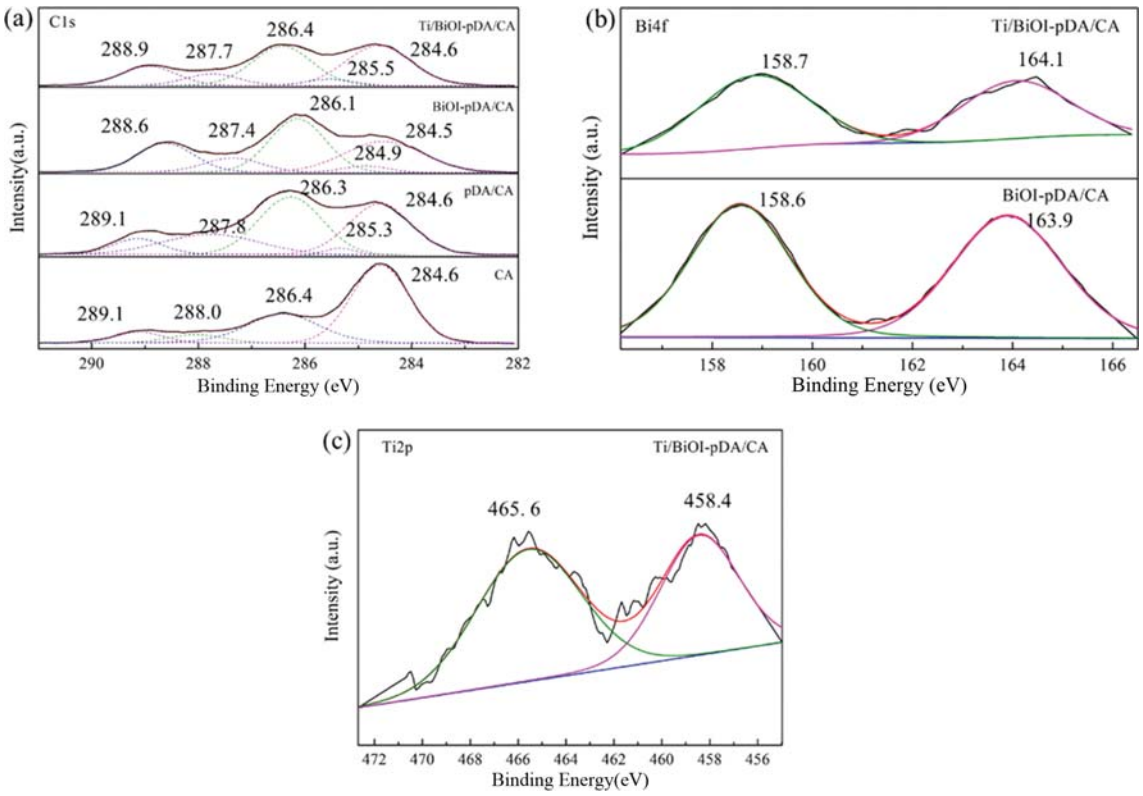

Fig. 5. XPS spectra of (a) C 1s peak, (b) Bi 4f peak and (c) Ti 2p peak of as-prepared membranes.

manifest that the Ti/BiOI photocatalyst had been successfully prepared.

2. Structural and Morphological Analyses of Membranes

The XRD patterns of pure and hybrid CA membranes are shown in Fig. 4(a). The only one major characteristic peak of original CA membranes detected at approximately 22.6° was consistent with previous reports [10]. For XRD patterns of hybrid CA membranes, new peaks were located at 2θ=29.6°, 31.7°, 39.4°, 45.7°, 51.3° and 55.2°, corresponding to the (102), (110), (004), (112), (200), (114) and (212) planes of BiOI, respectively, which means that the BiOI or Ti/BiOI photocatalyst immobilized into the original CA membranes. Interestingly, the diffraction peaks of BiOI and Ti/BiOI are also present in the XRD pattern of the pDA/CA membranes with lower intensity and smaller warp than that of pure CA membranes; this shift of peak position is due to the interaction of BiOI or Ti/BiOI with pDA. Therefore, the results illustrate that the BiOI or Ti/BiOI photocatalyst were successfully immobilized into the membranes.

The FT-IR spectra of pure and hybrid CA membranes are shown in Fig. 4(b). The characteristic peaks of pure CA membrane at 1,744, 1,371, 1,236 and 1,052 cm^{-1} are attributed to the stretching frequencies of C=O, C-CH_3, C-O-C and CH_2-OH, respectively. The broad band located at 3,000-3,700 cm^{-1} belongs to the intense stretching vibration of hydroxyl groups. However, with the pDA coating modification, blending BiOI and Ti/BiOI samples, the peak intensity of hydroxyl groups gradually became stronger. The result certified that pDA modified CA powder and hybrid membranes were successfully prepared. Therefore, the hydrophilicity of the membranes was improved by adding BiOI and Ti/BiOI, in accordance with the results of the water contact angle.

To understand the chemical composition of blank CA, pDA/CA, BiOI-pDA/CA and Ti/BiOI-pDA/CA membranes, XPS analysis was conducted. The XPS spectra of C 1s, Bi 4f and Ti 2p are presented in Fig. 5. As shown in Fig. 5(a), the peaks of the binding energies for blank CA membrane corresponding to C 1s are observed at 284.6 eV, 286.4 eV, 288 eV and 299.1 eV, which could be assigned to C-C or C-H, C-O, C=O and -O=C-O. Compaed with the pristine CA membrane, the existence of C-N bond in C 1s peak at 285.3 eV proves the formation of pDA on the surface of CA. After introducing the BiOI and Ti/BiOI, the peaks shifted in C 1s spectrum of BiOI-pDA/CA and Ti/BiOI-pDA/CA membranes, which may be due to the interaction between BiOI or Ti/BiOI and

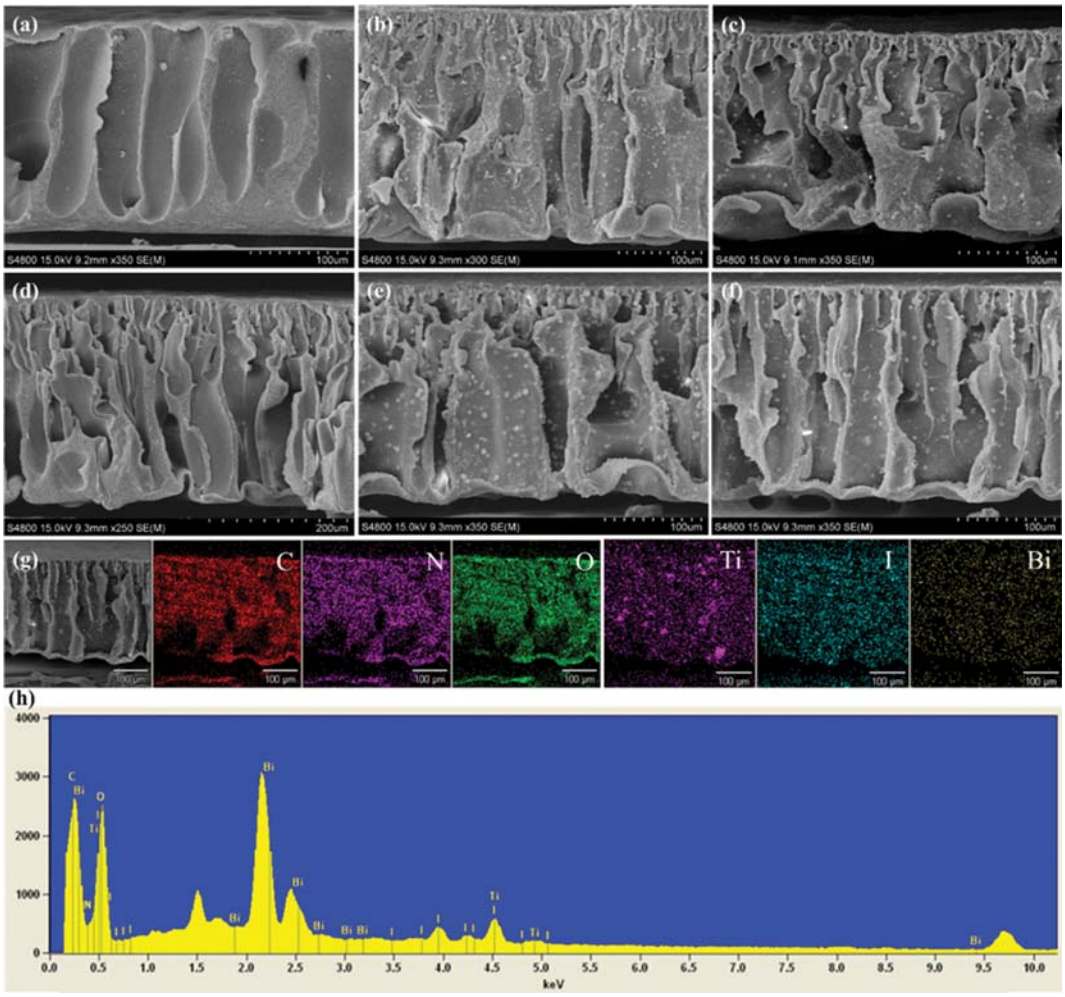

Fig. 6. SEM images of cross section morphology of (a) CA, (b) BiOI-CA, (c) Ti/BiOI-CA, (d) pDA/CA, (e) BiOI-pDA/CA, (f) Ti/BiOI-pDA/CA membranes and (g), (h) EDX mapping scanning spectrum.

pDA/CA. As for the Bi 4f XPS spectrum of BiOI-pDA/CA in Fig. 5(b), two peaks at 158.6 eV and 163.9 eV could be attributed to the Bi 4f 7/2 and Bi 4f 5/2 for the Bi^{3+}, respectively. However, these peaks slightly shifted to a higher binding energy for Ti/BiOI-pDA/CA, further indicating the strong interaction between Ti/BiOI and pDA/CA. Fig. 5(c) shows the peaks at 458.4 eV and 465.6 eV, which could be assigned to Ti 2p 3/2 and Ti 2p 1/2 peaks, respectively. The intensity of the Ti 2p spectrum was weak for the relatively low Ti content on the membrane surface. The above results indicate that the Ti/BiOI-pDA/CA membrane was successfully synthesized.

The cross-section morphology and pore size distribution of as prepared membranes are depicted in Fig. 6. All the membranes had porous asymmetric structures containing a thin dense skin layer and a finger-like porous supporting layer [47,49]. The rise of more pore channels in the finger-like supporting layer could be observed with the introduction of pDA and Ti/BiOI photocatalyst, which were related to the rapid mass transfer between solvent and non-solvent during the phase inversion process owing to the abundant hydrophilic groups of pDA, BiOI and Ti/BiOI photocatalyst. The porosity of the membranes in Table 2 suggests that the Ti/BiOI-pDA/CA membranes showed higher porosity than of the other five membranes [50], which was in agreement with the results of cross-section morphology of membranes. No agglomeration of Ti/BiOI photocatalyst could be seen in the cross-section images due to the uniform distribution of the Ti/BiOI photocatalyst in the casting solution. Furthermore, the SEM-EDX mapping scanning spectrum for Ti/BiOI-pDA/CA membranes was performed to further investigate the presence and dispersion uniformity of Ti/BiOI photocatalyst on the CA membrane surface. As shown in Fig. 6(g), (h), bismuth (Bi), oxygen (O), Iodine (I), titanium (Ti), carbon (C) and nitrogen (N) elements were observed, indicating the homogeneous dispersion of Ti/BiOI photocatalyst immobilized into pDA/CA membranes successfully.

AFM was used to examine the surface roughness of membranes, and the results are shown in Fig. 7 and Table 2. Ti/BiOI-pDA/CA membranes showed the highest surface roughness (41.0 nm) due to the presence of hydrophilic photocatalyst, which accelerates the mass transfer between solvent and non-solvent. The rapid solvent exchange could result in the formation of polymer nodules, which increase the surface roughness [51]. In addition, according to the previous work, high surface roughness is a way to improve the hydrophilic properties, and the relative rougher membrane surface is easy to contaminate. Although the incorporation of BiOI and Ti/BiOI in the polymeric membrane may cause potential membrane fouling, the fouling phenomenon could be covered by the degradation activity of the BiOI and Ti/BiOI itself. Therefore, this kind of membrane has been proven as an effective material to alleviate membrane fouling [17,52].

3. Filtration and Antifouling Performance of Membranes

Static BSA adsorption and water contact angle tests were car-

Table 2. Porosity, water contact angle, pure water flux, FRR and roughness parameters of various membranes

Membrane	Porosity (%)	Water contact angle (°)	Pure water flux (L m^2 h^{-1})	FRR	Roughness		
					Ra (nm)	Rq (nm)	Rz (nm)
CA	88.89	82	135.76	70.96	-	-	-
pDA/CA	89.92	78	168.64	70.78	20.5	27.1	7.01
BiOI-CA	90.18	75	218.46	72.07	-	-	-
BiOI-pDA/CA	90.57	74	259.10	82.78	33.6	44.8	14.0
Ti/BiOI-CA	90.37	70	229.22	74.62	-	-	-
Ti/BiOI-pDA/CA	91.70	69	294.80	87.92	41.0	60.3	17.5

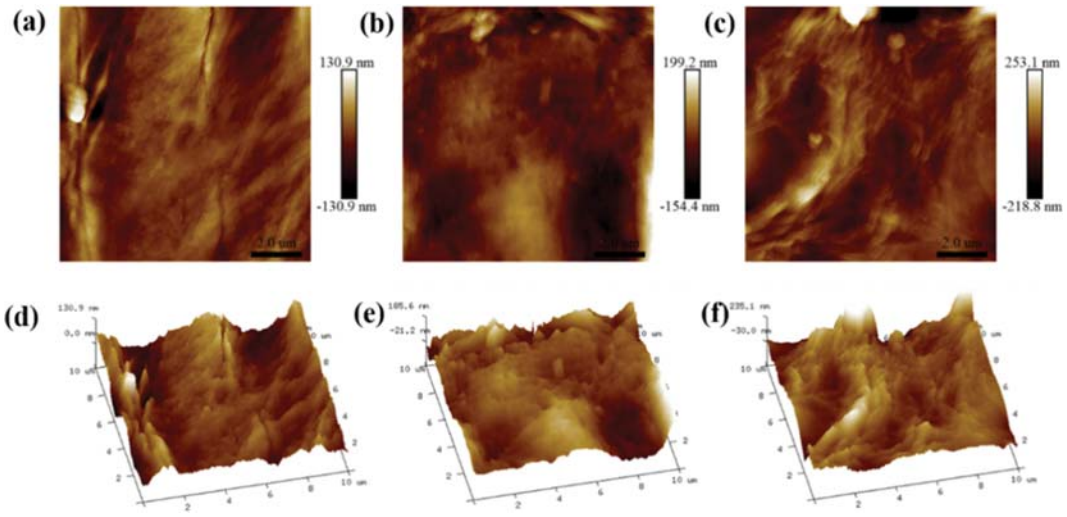

Fig. 7. AFM images of (a), (d) pDA/CA, (b), (e) BiOI/pDA/CA and (c), (f) Ti/BiOI-pDA/CA membranes.

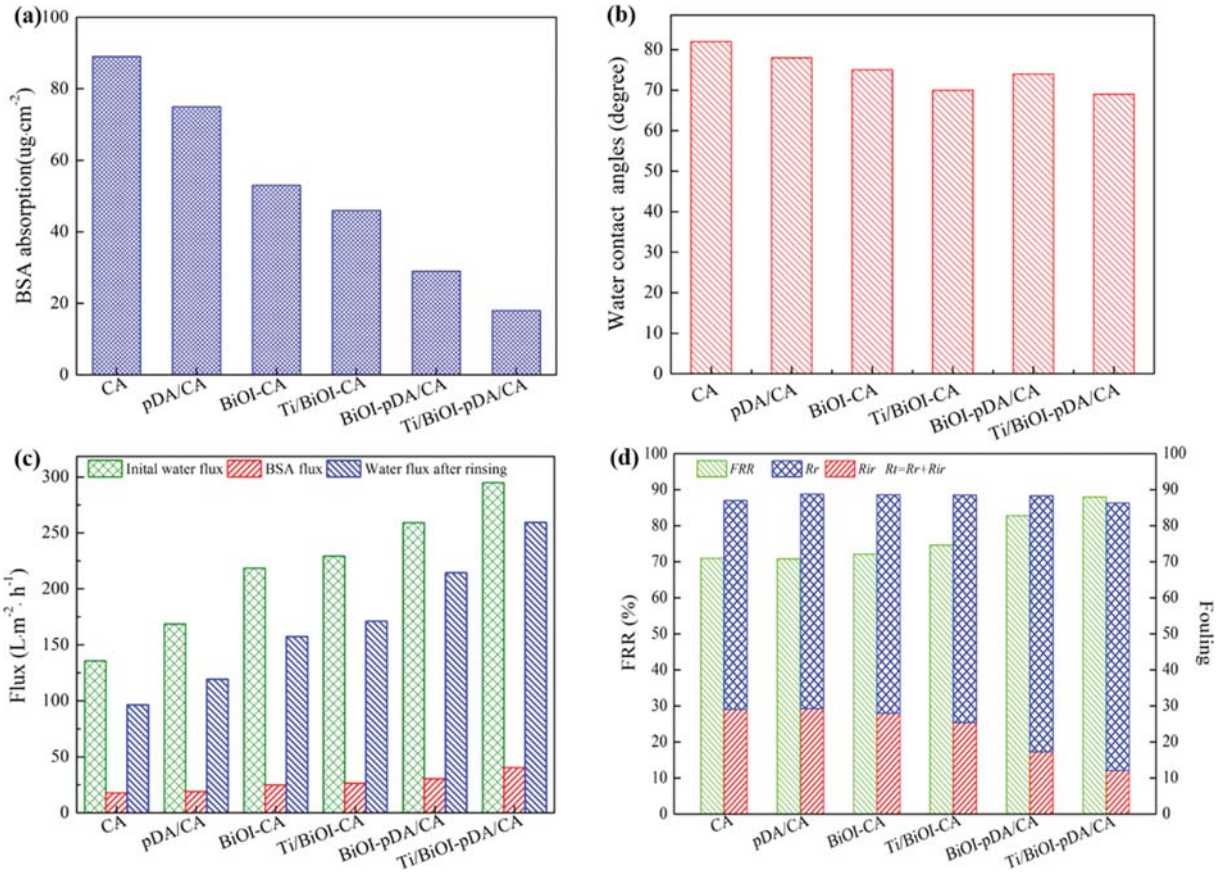

Fig. 8. (a) Static adsorption of BSA, (b) contact angle and pure water permeance, (c) equilibrium flux values at different process (fresh, after fouling and rinsing), (d) water flux recovery ratio (FRR), reversible fouling ratio (Rr), irreversible fouling ratio (Rir) and total fouling ratio (Rt, the sum of Rr and Rir) of the prepared membranes.

ried out to determine the fouling properties of the membranes. Fig. 8(a) shows that the BSA adsorption clearly decreases after blending inorganic nanomaterials into the pure polymer membrane matrix. Fig. 8(b) clearly shows that the water contact angle of the pDA/CA membrane was smaller than that of the original CA membrane due to the presence of hydroxyl and amino groups of pDA. The contact angle of Ti/BiOI-pDA/CA membrane decreased to 69° with the supplementation of Ti/BiOI photocatalyst. These results could be attributed to the spontaneous migration of hydrophilic nanoparticles to the membrane/water interface. The hydrophilic groups can easily form hydrogen bonds with water molecules, forming effective steric hindrance on the membrane surface and inhibiting the adhesion and deposition of pollutants on the membrane surface. Therefore, the special structure of the Ti/BiOI-pDA/CA membrane not only greatly increased the hydrophilicity of the membranes but also mitigated membrane fouling.

The pure water flux of various membranes was determined, and the results are illustrated in Table 2 and Fig. 8(c), From Table 2, the pure CA membranes clearly had the pure water flux value of 135.76 L·m^{-2}·h^{-1}, 168.64 L·m^{-2}·h^{-1} for pDA/CA, 259.10 L·m^{-2}·h^{-1} for BiOI-pDA/CA and 294.80 L·m^{-2}·h^{-1} for Ti/BiOI-pDA/CA membranes, respectively. This improvement in pure water flux may be attributed to the presence of hydroxyl groups on the pDA and photocatalytic surface, which decreased the interaction between the membrane surface and contaminants, then facilitated the water molecules to pass through the membrane. These results further indicated that the hybrid membranes had high hydrophilicity and anti-fouling property.

To comprehensively evaluate membrane fouling, FRR, Rr, Rir and Rt were calculated using Eqs. (5)-(8) through the water flux of hybrid membranes before and after filtration of 1.0 g L^{-1} BSA solution fouling and after the cleaning by rinsing with deionized water [51]. These values are presented in Fig. 8(c) and (d). It can be observed from Fig. 8(c) that the BSA flux of various membranes was improved, and Ti/BiOI-pDA/CA membranes had the highest BSA flux, which implied the improved antifouling performance of blending membranes. After rinsing with DI water, the water flux of membranes increased because of the removal of loosely bound BSA formed on the membrane surface. However, it could not regain the previous water flux owing to the inner pore blocking and irreversible adsorption of BSA. Fig. 8(d) shows that FRR of blending membranes was clearly higher than that of pure CA and pDA/CA membranes, indicating the enhancement of antifouling characteristic. The pristine CA and pDA/CA membranes displayed the FRR of 70.96% and 70.78%, implying a relatively poor antifouling property. With the addition of BiOI and Ti/BiOI into CA membranes, the FRR increased to 72.07% and 74.62%, respectively. While coupling BiOI and Ti/BiOI photocatalysts with pDA/CA membrane,

the FRR tended to considerably increase, and the maximum FRR value (87.92%) was observed for Ti/BiOI-pDA/CA membranes, which suggested that the amelioration of antifouling behavior could be ascribed to the more hydroxide groups on the surfaces of pDA and Ti/BiOI. The hydrophilic hydroxide groups could prevent the attachment of the foulant agent on the membrane surface [53]. Furthermore, Rt (Rt=Rr+Rir) values for hybrid membranes were slightly smaller than that of pure CA membrane. The lower Rt values indicated that the Ti/BiOI-pDA/CA membranes had higher water flux and better antifouling properties. The values of Rir clearly decreased, indicating that the adsorbed BSA on the hybrid membranes could be easily removed by simple cleaning with DI water. These observations suggest that blending photocatalyst into membranes could enhance membrane hydrophilicity and endow membrane with antifouling tendency.

4. Photocatalytic Activity of Membranes

The UV-vis absorption/diffusion spectra (DRS) were used to estimate the optical absorption properties of hybrid membranes. As can be seen from Fig. 9(a), the absorption intensity of pDA/CA hybrid membranes has larger enhancement in the whole visible region as compared to CA hybrid membranes due to the photosensitizer role of pDA. Moreover, Ti/BiOI-pDA/CA membranes show maximum absorption intensity in UV and visible region. Therefore, the above results of DRS demonstrate that pDA and Ti/BiOI play beneficial roles and could improve the absorption of visible light for photocatalytic degradation.

The photocatalytic activities of membranes were tested by removing TC aqueous solution (10 mg L^{-1}) under irradiation of a 300 W xenon light lamp. Typically, a piece of membrane was added into 50 mL of the TC solution with or without visible-light irradiation. Adsorption experiments of the different membranes for TC solution without visible-light irradiation were carried out. As described in Fig. 9(b), the removal ratio of CA and pDA/CA membranes for TC was 19% and 24% in 60 min. By supplementation of the CA and pDA/CA membrane matrix with BiOI and Ti/BiOI, the adsorption rate of BiOI-CA, Ti/BiOI-CA, BiOI-pDA/CA and Ti/BiOI-pDA/CA membranes was 28%, 36%, 29% and 38%, respectively. It was obvious that Ti/BiOI had superior adsorptive ability toward TC owing to its high specific surface area and strong adsorption capacity, which was beneficial to the photodecomposition of TC. Therefore, BiOI-CA membranes had 39% of photodegradation efficiency toward TC, 84% for Ti/BiOI-CA membranes within the same period under visible-light irradiation, suggesting that Ti doped BiOI could enhance the photocatalytic activity. However, photocatalytic activity of BiOI-pDA/CA and Ti/BiOI-pDA/CA membranes for TC was significantly improved under the same circumstances; the removal rates for BiOI-pDA/CA and Ti/BiOI-pDA/CA membranes were 52%, 98% under the visible-light irradiation, respectively. This could be attributed to the introduction of pDA; it not only reinforced light absorption but also effectively promoted the separation and transfer of carrier generation under visible-light irradiation [54].

To understand membrane photocatalytic performance in-depth, the degradation data can be further evaluated by pseudo-first-order equation $\ln(C_0/C)=kt$ (Fig. 9(c)). The apparent first-order rate constant k for optimal Ti/BiOI-pDA/CA membrane could reach 0.03214 min^{-1}, which was larger than CA membrane (0.00186 min^{-1}), pDA/CA membrane (0.00213 min^{-1}), BiOI/CA membrane (0.00391 min^{-1}), Ti/BiOI-CA membrane (0.00569 min^{-1}), BiOI/-pDA/CA membrane (0.01455 min^{-1}), respectively. The higher k could be

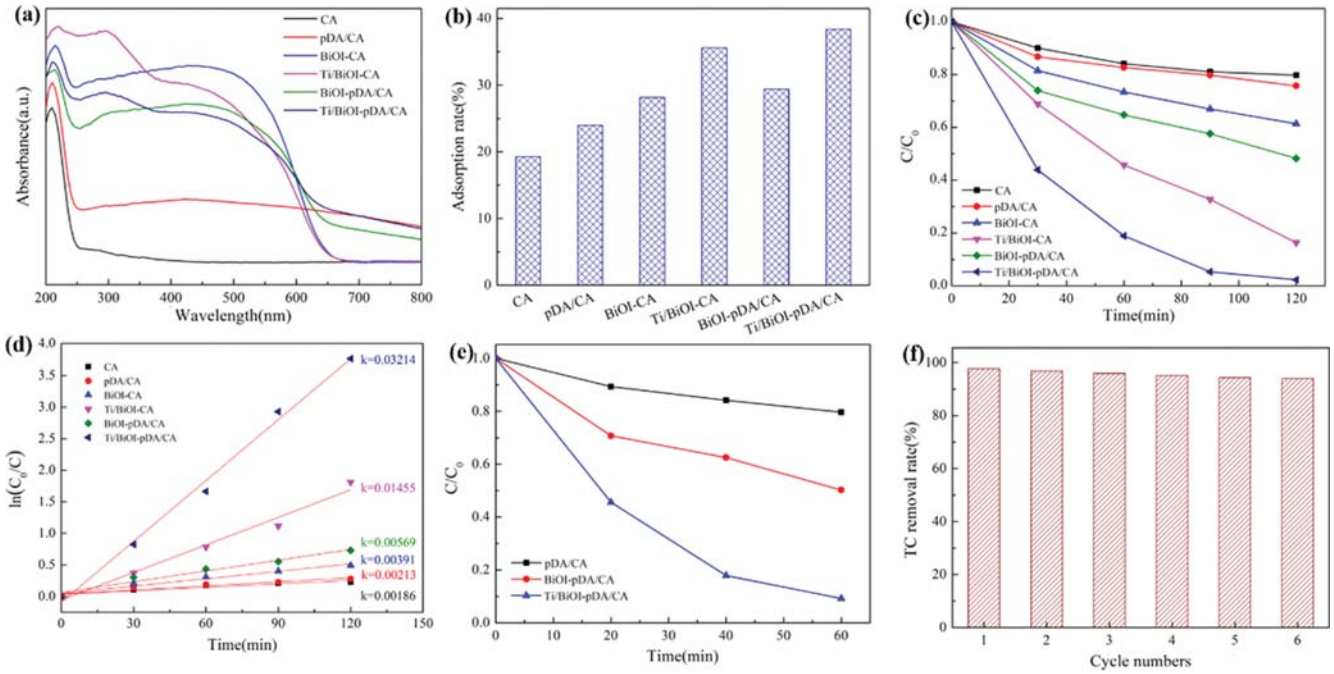

Fig. 9. (a) UV-vis diffuse reflectance spectra, (b) adsorption rate of different membranes without visible-light irradiation, (c) photocatalytic activity of different membranes, (d) the corresponding kinetic linear simulation curves, (e) dynamic cyclic photodegradation results and (f) cycling test and recyclability of Ti/BiOI-pDA/CA membranes.

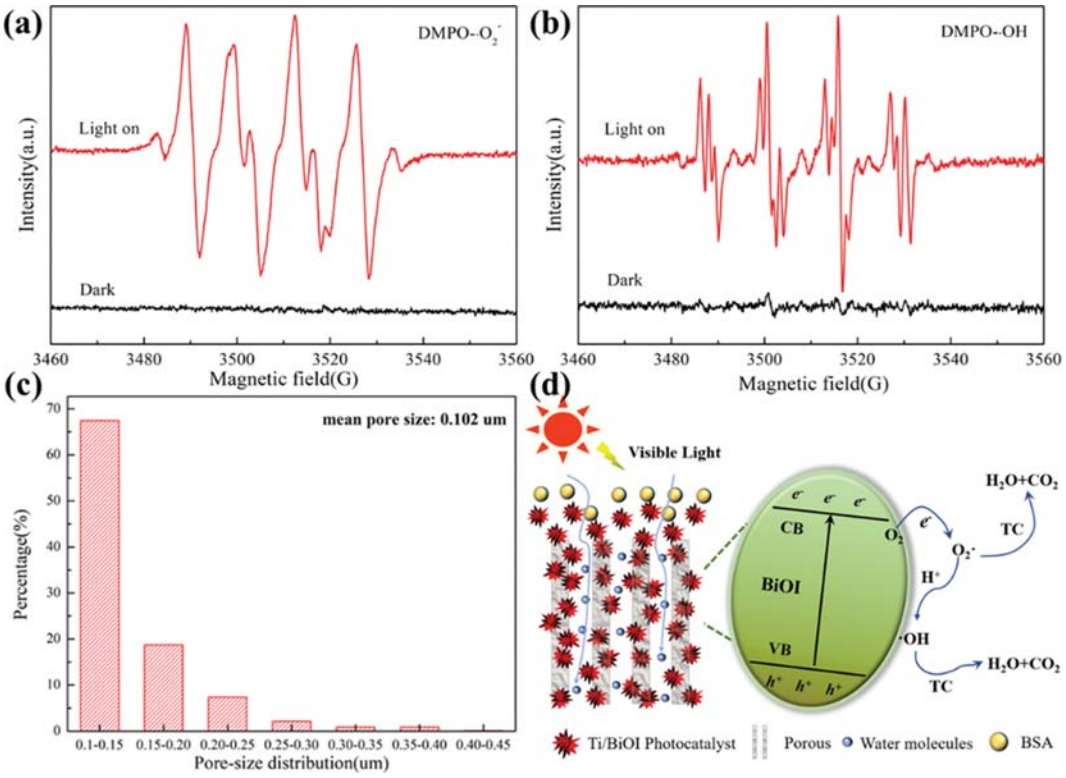

Fig. 10. ESR spectra of Ti/BiOI-pDA/CA membrane. (a) DMPO-$\cdot O^{2-}$ and (b) DMPO-·OH radical species; (c) pore size distribution of Ti/BiOI-pDA/CA membranes and (d) mechanism of photocatalytic degradation TC and antifouling over Ti/BiOI-pDA/CA membrane.

attributed to the fact that the Ti doping BiOI could reduce photogenerated electron hole pair recombination and eventually enhance the photocatalytic efficiency.

A sketch and results of dynamic cyclic degradation experiments are presented in Fig. 9(d) and (e), respectively. The concentration and volume of TC were the same as above static degradation condition. During every irradiation interval, about 5.0 mL TC solution was collected from photodegraded system. It can be seen from Fig. 9(e), the removal rate of Ti/BiOI/-pDA/CA membrane under dynamic cyclic degradation system was further improved as compared to that of static degradation experiment, and the TC removal efficiency reached 91% in 60 min higher than that of static degradation system. This might be attributed to the uniform distribution of Ti/BiOI on the surface or channels of the membrane, which increased the adsorption contact between TC and Ti/BiOI through fast transport to membrane surface, rather than diffusing in the dynamic cyclic degradation test [13,21].

The stability and recyclability of Ti/BiOI/-pDA/CA membrane were studied over repeating photocatalytic degradation of TC. For each recycling run, the photocatalytic membranes were washed with water for three times for the next catalytic experiment. As illustrated in Fig. 9(f), the removal efficiency of Ti/BiOI/-pDA/CA membrane was almost unchanged after sixth cycle experiments. This result indicated that the Ti/BiOI/-pDA/CA membrane was stable and could be readily reused for practical application.

5. Research on Antifouling and Photocatalytic Mechanism of the Membrane

The fouling mechanism of Ti/BiOI-pDA/CA membrane is summarized in Fig. 10(c), (d). The Ti/BiOI-pDA/CA membrane exhibited excellent super hydrophilic performance owing to the presence of hydroxyl groups of the Ti/BiOI photocatalyst and its high surface energy. When proteins and other foulants were poured onto Ti/BiOI-pDA/CA membrane surface, the membrane surface could bond with water molecules to form the hydrogen bond. Meanwhile, the water molecules could be arranged on the membrane surface with ordered structure to form a hydration layer, which could prevent the foulants permeating through the membrane surface, resulting in the enhancement of the antifouling activity. Furthermore, the pore size of Ti/BiOI-pDA/CA membrane was about 0.102 μm from Fig. 10(c); according to the additional pressure formula, the calculated Jurin height was about 280 m, which was much greater than the thickness of Ti/BiOI-pDA/CA membrane. Thus, the water molecules would remain continuously permeable under capillary action. Therefore, Ti/BiOI-pDA/CA membrane exhibited high antifouling activity.

ESR was applied to further detect the predominant active species over Ti/BiOI-pDA/CA membrane during the photocatalytic reaction process, including degradation and antifouling. As shown in Fig. 10, there are no ESR signals in the dark. However, the characteristic peaks of DMPO-$\cdot O^{2-}$ can be clearly detected in methanol (Fig. 10(a)) in the photocatalytic reaction system. Meanwhile, characteristic peaks of the DMPO-·OH are observed in water with visible light irradiation (Fig. 10(b)). Therefore, it is well suggested that the $\cdot O^{2-}$ and ·OH radicals are the main active species in the photocatalytic process.

Based on the above results, a possible photodegradation mecha-

nism of the Ti/BiOI-pDA/CA membranes for photocatalytic degradation is shown in detail in Fig. 10(d) and the following reactions. The •OH and O^{2-} are of high oxidation activity, which can further react directly with contaminants (TC or BSA on the membrane surface or the hole interior) to yield degradation products (CO_2 and H_2O).

$$Ti/BiOI+hv \rightarrow Ti/BiOI\ (e^- + h^+)$$
$$O_2 + e^- \rightarrow \cdot O_2^-$$
$$\cdot O_2^- + 2H^+ + e^- \rightarrow H_2O_2$$
$$H_2O_2 + e^- \rightarrow \cdot OH + {}^-OH$$
$$-OH + h^+ \rightarrow \cdot OH$$
$$\cdot OH + \cdot O_2^- + TC/BSA \rightarrow \text{degradation products}$$

CONCLUSIONS

Ti/BiOI-pDA/CA membranes were successfully fabricated by a facile phase inversion method. Owing to the attractive photocatalytic efficiency of Ti/BiOI under visible light irradiation, the Ti/BiOI-pDA/CA membrane displayed high performance for the removal of TC and superior antifouling activity. The obtained Ti/BiOI-pDA/CA membranes exhibited higher porosity and surface roughness compared with other membranes. Moreover, they showed dramatic improvement in pure water flux and hydrophilicity, resulting in increased antifouling property and separation performance. Rr, Rir and FRR also indicated that the Ti/BiOI-pDA/CA membranes possessed superior fouling resistance. Furthermore, Ti/BiOI-pDA/CA membrane exhibited stable and high photocatalytic degradation efficiency even after six cycles of use. These encouraging results provide experimental basis for further applications in tackling practical wastewater treatment.

ACKNOWLEDGEMENTS

This work was financially supported by the National Natural Science Foundation of China (No. 21806060, 21808089, 21776110), the Postgraduate Research & Practice Innovation Program of Jiangsu Province (No. KYCX19_1589), the Natural Science Foundation of Jiangsu Province (No. BK20171315, BK20181230, BK20180192), the China Postdoctoral Science Foundation (No. 1501067C, 170103B).

REFERENCES

1. J. J. Xue, S. S. Ma, Y. M. Zhou, Z. W. Zhang and M. He, *ACS Appl. Mater. Interfaces*, **7**, 9630 (2015).
2. J. Li, Y. Ma, Z. Ye, M. Zhou, H. Wang, C. Ma, D. Wang, P. Huo and Y. Yan, *Appl. Catal. B-Environ.*, **204**, 224 (2017).
3. J. Qiao, H. Zhang, G. Li, S. Li, Z. Qu, M. Zhang, J. Wang and Y. Song, *Sep. Purif. Technol.*, **211**, 843 (2019).
4. D. Wang, F. Jia, H. Wang, F. Chen, Y. Fang, W. Dong, G. Zeng, X. Li, Q. Yang and X. Yuan, *J. Colloid Interface Sci.*, **519**, 273 (2018).
5. Y. Yang, Z. T. Zeng, C. Zhang, D. L. Huang, G. M. Zeng, R. Xiao, C. Lai, C. Y. Zhou, H. Guo, W. J. Xue, M. Cheng, W. J. Wang and J. J. Wang, *Chem. Eng. J.*, **349**, 808 (2018).
6. J. Y. Cao, L. D. Lai, B. Lai, G. Yao, X. Chen and L. P. Song, *Chem. Eng. J.*, **364**, 45 (2019).
7. A. Xie, J. Dai, J. Cui, J. Lang, M. Wei, X. Dai, C. Li and Y. Yan, *ACS Sustain. Chem. Eng.*, **5**, 11566 (2017).
8. B. Dai, H. Huang, F. Wang, C. Lu, J. Kou, L. Wang and Z. Xu, *Chem. Eng. J.*, **347**, 263 (2018).
9. W. Xing, Y. Wu, C. Li, J. Lu, X. Lin and C. Yu, *ACS Sustain. Chem. Eng.*, **8**, 5636 (2020).
10. H. Younas, H. Bai, J. Shao, Q. Han, Y. Ling and Y. He, *J. Membr. Sci.*, **541**, 529 (2017).
11. K. G. Mu, D. L. Zhang, Z. Q. Shao, D. J. Qin, Y. L. Wang and S. Wang, *Carbohydr. Polym.*, **174**, 688 (2017).
12. R. Zhu, A. J. Diaz, Y. Shen, F. Qi, X. Chang, D. P. Durkin, Y. Sun, S. D. Solares and D. Shuai, *J. Membr. Sci.*, **563**, 531 (2018).
13. B. Li, M. Meng, Y. Cui, Y. Wu, Y. Zhang, H. Dong, Z. Zhu, Y. Feng and C. Wu, *Chem. Eng. J.*, **365**, 405 (2019).
14. W. Li, B. Li, M. Meng, Y. Cui, Y. Wu, Y. Zhang, H. Dong and Y. Feng, *Appl. Surf. Sci.*, **487**, 1008 (2019).
15. J. Lu, Y. Wu, X. Lin, J. Gao, H. Dong, L. Chen, Y. Qin, L. Wang and Y. Yan, *J. Hazard. Mater.*, **353**, 244 (2018).
16. J. Cui, Z. Zhou, A. Xie, Q. Wang, S. Liu, J. Lang, C. Li, Y. Yan and J. Dai, *J. Membr. Sci.*, **573**, 226 (2019).
17. T. Wang, Z. Wang, P. Wang and Y. Tang, *J. Membr. Sci.*, **572**, 419 (2019).
18. Z. Xu, T. Wu, J. Shi, K. Teng, W. Wang, M. Ma, J. Li, X. Qian, C. Li and J. Fan, *J. Membr. Sci.*, **520**, 281 (2016).
19. Y. Zhang, Q. Li, Q. Gao, S. Wan, P. Yao and X. Zhu, *Appl. Catal. B-Environ.*, **267**, 118715 (2020).
20. D. Y. Koseoglu-Imer, B. Kose, M. Altinbas and I. Koyuncu, *J. Membr. Sci.*, **428**, 620 (2013).
21. X. Fang, J. Li, B. Ren, Y. Huang, D. Wang, Z. Liao, Q. Li, L. Wang and D. D. Dionysiou, *J. Membr. Sci.*, **579**, 190 (2019).
22. D. Chen, J. Yang, Y. Zhu, Y. Zhang and Y. Zhu, *Appl. Catal. B-Environ.*, **233**, 202 (2018).
23. J. Zhang, J. Fu, Z. Wang, B. Cheng, K. Dai and W. Ho, *J. Alloys Compd.*, **766**, 841 (2018).
24. H. Che, C. Liu, W. Hu, H. Hu, J. Li, J. Dou, W. Shi, C. Li and H. Dong, *Catal. Sci. Technol.*, **8**, 622 (2018).
25. N. Han, Y. Wang, H. Yang, J. Deng, J. Wu, Y. Li and Y. Li, *Nat. Commun.*, **9**, 1320 (2018).
26. Z. Jiang, X. Liang, Y. Liu, T. Jing, Z. Wang, X. Zhang, X. Qin, Y. Dai and B. Huang, *Appl. Catal. B-Environ.*, **211**, 252 (2017).
27. L. Zeng, F. Zhe, Y. Wang, Q. L. Zhang, X. Y. Zhao, X. Hu, Y. Wu and Y. M. He, *J. Colloid Interface Sci.*, **539**, 563 (2019).
28. L. Yosefi and M. Haghighi, *Appl. Catal. B-Environ.*, **220**, 367 (2018).
29. X.-J. Wen, C.-G. Niu, L. Zhang, C. Liang and G.-M. Zeng, *J. Catal.*, **356**, 283 (2017).
30. R. A. He, K. Y. Cheng, Z. Y. Wei, S. Y. Zhang and D. F. Xu, *Appl. Surf. Sci.*, **465**, 964 (2019).
31. B. J. Dai, A. C. Zhang, Z. Y. Liu, T. T. Wang, C. W. Li, C. J. Zhang, H. X. Li, Z. C. Liu and X. M. Zhang, *Catal. Commun.*, **121**, 53 (2019).
32. J. Liang, J. Deng, M. Li, T. Xu and M. Tong, *Colloid Surf. B-Biointerfaces*, **147**, 307 (2016).
33. Y. L. Wu, J. Lu, X. Y. Lin, J. Gao, L. Chen, J. Y. Cui, P. Lv, X. L. Liu, M. J. Meng and Y. S. Yan, *ACS Sustain. Chem. Eng.*, **6**, 9104 (2018).
34. X. Wu, Y. Wu, L. Chen, L. Yan, S. Zhou, Q. Zhang, C. Li, Y. Yan and H. Li, *J. Membr. Sci.*, **553**, 151 (2018).

35. J.-H. Li, X.-X. Ni, D.-B. Zhang, H. Zheng, J.-B. Wang and Q.-Q. Zhang, *Appl. Surf. Sci.*, **444**, 672 (2018).
36. K. Cui, B. Yan, Y. Xie, H. Qian, X. Wang, Q. Huang, Y. He, S. Jin and H. Zeng, *J. Hazard. Mater.*, **350**, 66 (2018).
37. C. Wang, Y. L. Wu, J. Lu, J. Zhao, J. Y. Cui, X. L. Wu, Y. S. Yan and P. W. Huo, *ACS Appl. Mater. Interfaces*, **9**, 23687 (2017).
38. H. Wu, Y. Liu, L. Mao, C. Jiang, J. Ang and X. Lu, *J. Membr. Sci.*, **532**, 20 (2017).
39. P. Xia, M. Liu, B. Cheng, J. Yu and L. Zhang, *ACS Sustain. Chem. Eng.*, **6**, 8945 (2018).
40. L. Guo, Q. Liu, G. Li, J. Shi, J. Liu, T. Wang and G. Jiang, *Nanoscale*, **4**, 5864 (2012).
41. W. Xiong, X. Y. Li, Q. D. Zhao, Y. Shi and C. Hao, *J. Hazard. Mater.*, **359**, 186 (2018).
42. D. Yang, Y. Y. Sun, Z. W. Tong, Y. Tian, Y. B. Li and Z. Y. Jiang, *J. Phys. Chem. C*, **119**, 5827 (2015).
43. N. Nie, F. He, L. Zhang and B. Cheng, *Appl. Surf. Sci.*, **457**, 1096 (2018).
44. S.-R. Zhu, Q. Qi, W.-N. Zhao, M.-K. Wu, Y. Fang, K. Tao, F.-Y. Yi and L. Han, *Dalton Trans.*, **46**, 11451 (2017).
45. F. He, G. Chen, Y. Yu, Y. Zhou, Y. Zheng and S. Hao, *Chem. Commun.*, **51**, 6824 (2015).
46. M. Safarpour, A. Khataee and V. Vatanpour, *Sep. Purif. Technol.*, **140**, 32 (2015).
47. Y. Cui, L. Yang, M. Meng, Q. Zhang, B. Li, Y. Wu, Y. Zhang, J. Lang and C. Li, *Korean J. Chem. Eng.*, **36**, 236 (2019).
48. W. Zhang, W. Cheng, E. Ziemann, A. Be'er, X. Lu, M. Elimelech and R. Bernstein, *J. Membr. Sci.*, **565**, 293 (2018).
49. M. Safarpour, V. Vatanpour and A. Khataee, *Desalination*, **393**, 65 (2016).
50. H. Xu, M. Ding, W. Chen, Y. Li and K. Wang, *Sep. Purif. Technol.*, **195**, 70 (2018).
51. A. Abdel-Karim, S. Leaper, M. Alberto, A. Vijayaraghavan, X. Fan, S. M. Holmes, E. R. Souaya, M. I. Badawy and P. Gorgojo, *Chem. Eng. J.*, **334**, 789 (2018).
52. M. A. Mohamed, W. N. W. Salleh, J. Jaafar, A. F. Ismail, M. A. Mutalib, N. A. A. Sani, S. E. A. M. Asri and C. S. Ong, *Chem. Eng. J.*, **284**, 202 (2016).
53. L. Ghalamchi, S. Aber, V. Vatanpour and M. Kian, *Sep. Purif. Technol.*, **226**, 218 (2019).
54. Z. Yu, F. Li, Q. Yang, H. Shi, Q. Chen and M. Xu, *ACS Sustain. Chem. Eng.*, **5**, 7840 (2017).

APPENDIX A: ABBREVIATIONS TABLE

Nomenclature

T	: time
S	: area
C	: concentration
R^2	: correlation coefficient
^oC	: degree centigrade
g	: gram
h	: hour
mg	: milligram
mL	: milliliter
FRR	: flux recovery ratio
V	: volume
J	: flux
Rt	: total fouling ratio
Rr	: reversible fouling ratio
Rir	: irreversible fouling ratio

APPENDIX B: ABBREVIATIONS TABLE

Nomenclature

DMSO	: dimethyl sulfoxide
BiOI	: bismuth oxyiodide
TC	: tetracycline
pDA	: polydopamine
CA	: cellulose acetate
SEM	: scanning electron microscopy
AFM	: atomic force microscope
DRS	: UV-vis absorption/diffuse spectra
FT-IR	: fourier infrared spectrum
XPS	: X-ray photoelectron spectroscopy
XRD	: X-ray diffraction
ESR	: electron spin resonance